

Automated tuning and characterization of a single-electron transistor charge sensor

A. Paurevic^{1,2}, A. Sakr³, T. Joshi^{1,5}, D. van der Bovenkamp³, Q. T. Nicolau³, F. A. Zwanenburg³, J. Baugh^{1,2,4,6}‡

¹) Institute for Quantum Computing, University of Waterloo, Waterloo N2L 3G1, Canada

²) Department of Physics, University of Waterloo, Waterloo N2L 3G1, Canada

³) MESA+ Institute for Nanotechnology, University of Twente, PO Box 217, 7500 AE Enschede, The Netherlands

⁴) Department of Chemistry, University of Waterloo, Waterloo N2L 3G1, Canada

⁵) Department of Electrical and Computer Engineering, University of Waterloo, Waterloo N2L 3G1, Canada

⁶) Waterloo Institute for Nanotechnology, University of Waterloo, Waterloo N2L 3G1, Canada

E-mail: baugh@uwaterloo.ca

Abstract. We present an automated protocol for tuning single-electron transistors (SETs) or single-hole transistors (SHTs) to operate as precise charge sensors. Using minimal device-specific information, the protocol performs measurements to enable the selection and ranking of high-sensitivity operating points. It also characterizes key device parameters, such as dot radius and gate lever arms, through acquisition and analysis of Coulomb diamonds. Demonstration on an accumulation-mode silicon SET at 1.5 K highlights its potential in the 1-2 K range for “hot” spin qubits in scalable quantum computing systems. This approach significantly reduces the tuning time compared to manual methods, with future improvements aimed at faster runtimes and dynamic feedback for robustness to charge fluctuations.

Keywords: single-electron transistor, charge sensor, metal-oxide-semiconductor, automated tuning

‡ Author to whom any correspondence should be addressed.

1. Introduction

Single-electron transistors (SETs) have demonstrated significant utility as precise charge sensors in various fields such as quantum devices, metrology, and fundamental physics. Specific applications include charge and spin state readout in semiconductor spin qubits, for which radio-frequency SETs (RF-SETs) have shown particular effectiveness for fast, high-fidelity readout [1, 2]. Other examples include realization of quantum current standards [3], and detection of fractional charge excitations in the fractional quantum Hall effect [4]. In order to act as a charge sensor, an SET must be tuned to an operating point where it is highly sensitive to changes in its surrounding electrostatic environment; this holds true for RF-SETs as well, which require DC tuning prior to RF operation. While this tuning can be done heuristically, there have been recent efforts to automate the tuning process of SETs, and semiconductor quantum dot devices in general, in order to speed up experiments and improve reliability [5].

Different automation protocols have targeted various phases of the tuning process, often focusing on tuning quantum dots for operation as spin qubits. Some techniques [6, 7] place emphasis on initialization of devices following cool-down, which encompasses establishing a suitable range of gate voltages for two-dimensional electron gas (2DEG) formation, tunnel barrier pinch-off, and forming the desired number of quantum dots in the system. Further tuning would then involve adjusting the number of charges on each dot as desired [8-10], in addition to setting up virtual gating, and fine tuning the dots and sensors for operating qubits [11, 12].

Beyond electron-based spin qubits, there is growing interest in ambipolar devices which make use of both SETs and single-hole transistors (SHTs), due to the potential advantages of hole quantum dots as spin qubits. Notably, the large spin-orbit coupling of holes would enable efficient manipulation of hole spin states using electric dipole spin resonance (EDSR) [13, 14]. Large spin-orbit coupling would, however, make holes less suited for shuttling as compared to electrons [15], motivating the potential use of both charge carriers in a single system, where holes can be fixed in place and electrons can be shuttled. Ambipolar devices allow for characterizing both electron and hole quantum dots simultaneously and for direct comparison between them. As demonstrated by Sousa de Almeida *et. al.* [16], adjacent SET and SHT structures can be used for mutual sensing, which requires tuning one device as a charge sensor for the other. Using an automated tuning protocol that works for both n- and p-type devices could allow for seamless transition between operating and sensing regimes of the two structures.

In this work, we present a protocol [17] that can tune both electron- and hole-based devices to operate as precise charge sensors. The protocol initializes devices after cool-down with no prior experimental information, and determines several key characteristics of the sensor, such as the estimated dot radius and gate lever arms based on analysis of Coulomb diamonds. We demonstrate operation of the protocol for an accumulation mode SET device at a temperature of 1.5 K, where the device is sufficiently compact to allow its charging energy to exceed the thermal energy scale. This showcases the effectiveness of the protocol in the 1-2 K temperature range, where “hot” spin qubits are expected to be operated in future large-scale quantum computing devices [18].

2. Experimental Setup

The automated tuning protocol is demonstrated on a silicon metal-oxide-semiconductor (MOS) SET cooled to 1.5 K in a pumped helium-4 (^4He) cryostat. Figure 1 shows a schematic of the experimental setup. The SET has two layers of gate electrodes, separated by a dielectric. The accumulation gate A (top layer) induces a 2DEG, as it overlaps with degenerately doped (n^{++}) regions formed by shallow ion implantation far from the active device area that act as Ohmic contacts. In the device region, the induced 2DEG is locally depleted by barrier gates B1 and B2 (bottom layer) to form tunneling barriers. A quantum dot is thus formed between the two barrier gates, with its electrochemical potential tuned by the plunger gate P.

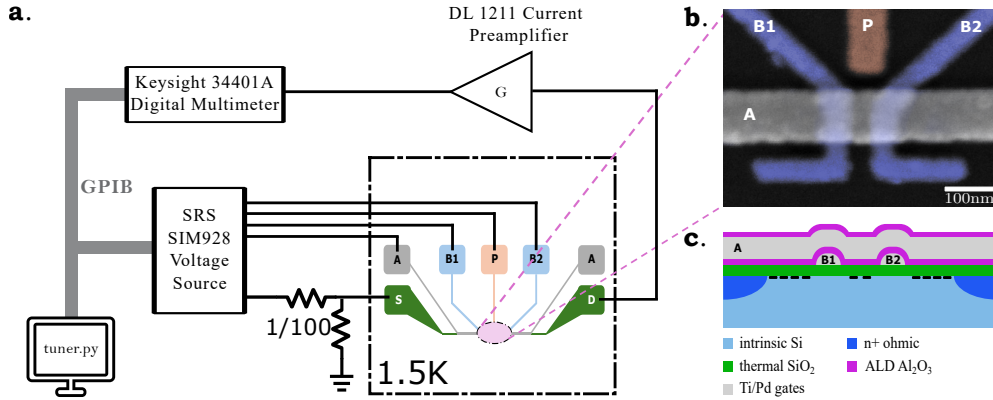


Figure 1. (a) Schematic of the experimental setup. The device is held at 1.5 K in a pumped ^4He cryostat. The computer, DC voltage source and digital multimeter are connected via GPIB. A Python script on the computer controls the DC source, applying appropriate voltages to the gates and the source-drain contacts of the device. The source-drain current is read by a current-voltage preamplifier fed into the digital multimeter. The preamplifier gain (G) is typically in the range of $10^7 - 10^8$ V/A. The computer acquires data from the multimeter, with the script implementing the automated tuning protocol. (b) False-color scanning electron micrograph (top view) and (c) schematic cross-section (side view) of the SET device. The Ti/Pd gate electrodes are deposited by electron-beam physical vapor deposition. Separating the barrier gates B1 and B2 from the top accumulation gate A is a 5 nm film of Al_2O_3 deposited by atomic layer deposition. The 2DEG forms in intrinsic (undoped) silicon, below 10 nm of thermally grown SiO_2 .

All DC voltages are supplied by SIM928 Isolated Voltage Sources (Stanford Research Systems) assembled on a SIM900 mainframe and controlled by the computer through GPIB signals. A source-drain DC voltage of $100 \mu\text{V}$ is applied to the device through a voltage divider. The current in the SET is measured by a Model 1211 Current Preamplifier (DL Instruments). The output voltage of the current preamplifier is read by a Keysight 34401A Digital Multimeter, which communicates the acquired data to the computer.

3. The Tuning Protocol

The tuning protocol we employ consists of three main stages: initialization, bias point selection, and sensitivity tuning, as depicted in Figure 2. In the first stage, all gate

voltages are swept from zero simultaneously until global turn-on is established (to positive/negative voltages for a SET/SHT). The two barrier gates are then individually swept back toward zero to verify that they can pinch-off the 2DEG/2DHG and to characterize any gating asymmetry. Following this stage, a two-dimensional scan of current versus the two barrier gates is obtained, varying the barrier gate voltages around their pinch-off values. Coulomb oscillations are detected and operating voltage values for B1 and B2 are selected to form the “bias point” (V_{B1}, V_{B2}). In the last stage of the protocol, the plunger gate is swept with the barrier gates fixed at the selected bias point, yielding a one-dimensional trace of Coulomb oscillations. Conductance peaks are identified and sorted into groups of high, medium, and low sensitivity. The following subsections describe each stage in detail, demonstrating operation of the protocol on an SET device.

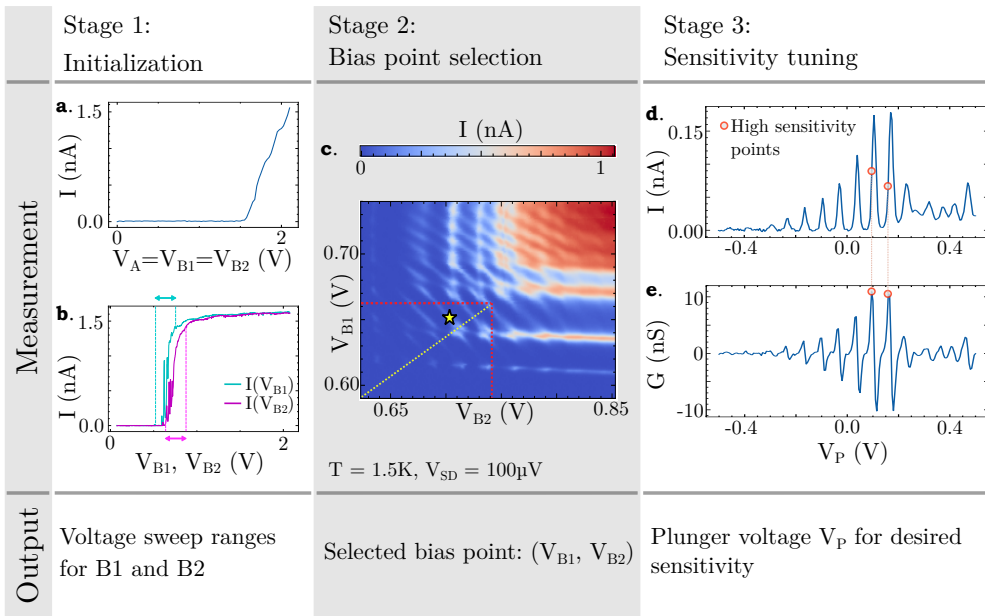


Figure 2. Overview of the autotuning protocol demonstrated on a SET. Stage 1 involves (a) increasing all gate voltages from zero until global turn-on is established, followed by (b) lowering barrier gate voltages separately to determine the voltage ranges where pinch-off occurs. A certain width around the pinch-off area is determined as the output of stage 1, as indicated by the blue and magenta arrows. (c) In stage 2, a 2D current-voltage measurement is performed using half of the barrier gate voltage ranges determined in stage 1. This region is shown within the red dotted lines, and is the standard range used when running the protocol. A 2D sweep over the complete pinch-off width determined in stage 1 is shown in panel (c) for clarity. A bias point on a Coulomb oscillation line is selected using image analysis, as indicated by the yellow star, while ensuring close proximity to the diagonal yellow line in order to maintain tunnel barrier symmetry. (d) In the last stage, the plunger gate voltage is swept while keeping the barrier gates fixed at this bias point in order to observe Coulomb oscillations. (e) The transconductance $G = dI/dV_P$ is calculated and peaks are identified and sorted into one of three categories of sensitivity. The two highest sensitivity points detected in this measurement are marked in red.

3.1. Initialization

The first step of the initialization stage is the grounding of all gates, and applying a small source-drain voltage to the ohmic contacts of the SET, a typical value for which is $100 \mu\text{V}$. This is followed by verifying that a current channel can form in the device by sweeping all gate voltages up (down) until a 2DEG (2DHG) accumulates. The sweep is halted when a preset current threshold is met. When implementing the protocol on the SET device described in Section 2 (see Figure 2(a)), this is set at $I_{\text{th}} = 1.5 \text{ nA}$. If the current never reaches the threshold value, the sweep is halted at a preset maximum allowed gate voltage. Failure to reach the current threshold for reasonable V_{SD} values indicates an unusable device, resulting in the device being rejected.

After global turn-on, the next step involves determining whether the barrier gates can pinch-off the device current. Failure of a barrier gate to do so due to electrostatic discharge damage or gate misalignment, for example, warrants rejection of the device from further tuning as it would not be usable as a SET. In order to perform this check, the two barrier gate voltages are independently swept downwards from the maximum gate voltage reached during global turn-on. The sweeps are terminated when either the current through the device falls below a minimum threshold, indicating successful pinch-off, or when a preset maximum differential voltage is met.

An example of this measurement is shown in Figure 2(b), where both barrier gate sweeps are overlaid. The main output of the first stage, as indicated in Figure 2, are the voltage ranges for each barrier around which pinch-off occurs. The data are fit to the logistic function $I(V) = I_0 + \frac{I_{max} - I_0}{1 + e^{-b(V - V_0)}}$, where I_{max} is the maximum current, V_0 is the inflection point of the sigmoidal curve, and the parameter b characterizes its steepness. The region within $V_0 \pm \frac{\sqrt{8}}{b}$ corresponds to the pinch-off width and is the voltage range of interest. Limiting the barrier-barrier sweep in Stage 2 to within this range ensures that the device is operated in a safe regime where a quantum dot is expected to form, since tunneling and confinement occur near pinch-off. Coulomb oscillations (sharp features in current) can be seen near pinch-off for both barrier sweeps in Figure 2(b).

3.2. Bias point selection

The second stage of the tuning protocol entails a two-dimensional current-voltage measurement in which both barrier gates are swept within small ranges around pinch-off, as determined by the output of stage 1. When running the protocol during a regular tuning process, only half of the pinch-off ranges from stage 1 are used. Each barrier voltage is varied from the minimum ($V_0 - \frac{\sqrt{8}}{b}$) to the center (V_0) value of the pinch-off range of interest. An example measurement depicting a sweep of the full pinch-off range is shown in Figure 2(c) where Coulomb oscillations are observed as diagonal lines appearing in the middle to lower left of the figure, bordered by the dotted red lines which represent the center values (inflection points of the fitted sigmoidal curves). These diagonal lines are identified as Coulomb oscillations of the intended SET quantum dot. Note that there are also horizontal and vertical features that likely arise from unintended regions of confinement below the barrier gates.

The angle of the diagonal lines relative to the horizontal depends on the ratio of capacitive coupling of the dot to the source and drain, respectively. Since it is observed to be close to 45° in this example, it can be inferred that the quantum dot formed

symmetrically between the two barriers. In order for the protocol to select a suitable bias point, it first performs a Hough transform on the barrier-barrier sweep to detect the Coulomb oscillations. Based on the symmetry of the barrier gates observed in Stage 1, the lines are filtered for suitable angles. For example, for relatively symmetric barriers, as depicted in Figure 2, angles are restricted between 40° and 50° . Any point on a line with a suitable angle within the sweep can thus be selected as the device bias point. The protocol outputs a number of options corresponding to appropriate lines, selecting a point near the indicated diagonal yellow line such that the tunnel barriers remain fairly symmetric. A user selects one of the bias points proposed by the protocol before proceeding with stage 3.

3.3. Sensitivity tuning

The final stage of the autotuning protocol is to perform a sweep of the plunger gate voltage at the bias point selected in stage two. This results in a 1D trace exhibiting Coulomb oscillations in current if a quantum dot has successfully formed. An empirically determined range is first used for the plunger gate sweep, a reasonable example for which is -0.5 V to 0.5 V. The protocol can adjust this range based on a desired number of Coulomb oscillations using peak extraction. A low-pass filter is applied to the current trace for smoothing, and its derivative is calculated numerically in order to obtain the transconductance $G = dI/dV_P$ as a function of the plunger voltage. Peaks in the transconductance are then detected and sorted based on their magnitude into three different categories: high, medium, and low sensitivity.

High sensitivity points are typically used for charge sensing. An application that also uses low sensitivity points is noise spectroscopy, where the gate voltages are held constant and the device current is recorded for many time points [19-21]. A Fourier transform of this time domain data reveals the frequency characteristics of the noise. Spectrograms taken for plunger voltages that correspond to high and low sensitivities can be compared in order to identify potential sources of noise in the system. Intrinsic noise originating from the electrostatic environment of the device would be detected with greater amplitude at a high sensitivity point, whereas noise from the measurement setup or cable pickup, for example, would be consistent for both high and low sensitivity points.

3.4. Coulomb Diamond Analysis

In addition to tuning, the protocol has been extended to the automated characterization of SET/SHT devices. Key device parameters can be determined by analyzing Coulomb diamonds, wherein both the plunger and source-drain voltages are varied to generate a 2D dataset, as depicted in Figure 3 (a). This sweep is performed at the bias point determined in stage 2 of the tuning protocol, at which a central dot is formed. The range of plunger voltages in the sweep is based on that used in stage 3 of the protocol when performing the Coulomb oscillation trace, limiting the range to contain a certain number of detected peaks. To establish the sweep range for the source-drain voltage, a value is estimated based on the charging energy of a circular dot, the diameter of which is equal to the distance between the two barrier gates. A buffer of 25 % is added to account for variations in dot size, and the exact value used can be manually adjusted if needed.

To automatically detect and analyze the diamonds, the data is first filtered by

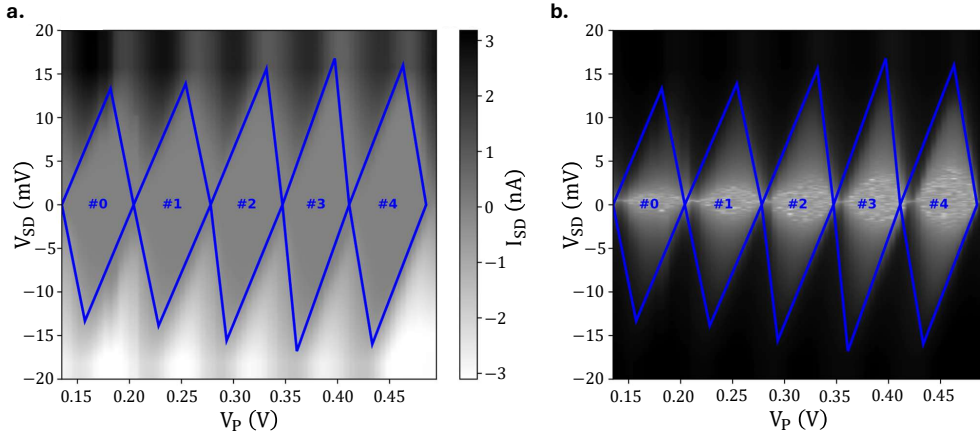


Figure 3. Coulomb diamonds measured at $T = 1.5$ K, with detected edges overlaid in solid blue lines. **(a)** Source-drain current I_{SD} plotted against the plunger gate voltage (V_P) and source-drain voltage (V_{SD}). **(b)** Detected diamond edges plotted over $\log(|I_{SD}|)$, which is the main quantity used to determine the edge positions.

taking the logarithm of the current and applying a mask based on the preset binary threshold used to determine the source-drain voltage range. This results in an image where each pixel corresponds to one of two distinct values. With a suitable binary threshold, all points within the diamond regions correspond to one value, and all points outside correspond to the other. A Gaussian blur is then applied to the image in order to smooth the edges and reduce noise. The image is segmented by a horizontal line going through the diamond midpoints, and a Hough transform is performed on each of the two segments to detect the diamond edges. The dimensions and slopes of the edges are estimated, and slopes from the two image segments that correspond to parallel edges within a single diamond are averaged. Fits to the diamonds are plotted based on the intersection points of their edges. Figure 3 **(b)** shows the detected diamonds overlaid on $\log(|I_{SD}|)$, highlighting the clarity in distinguishing the diamond shapes when using the logarithm of the current. A slight misalignment in the detected diamond intersection points can mainly be attributed to the low resolution of the image used; a voltage sweep with finer spacing would yield higher resolution and thus more accurate lines detected by the Hough transform. The fits also vary slightly depending on the choice of the binary threshold.

Through this analysis, we estimate several key parameters of the SET, as shown in Table 1. The lever arm α is given by the ratio of the half height and the width of a Coulomb diamond. The addition voltage, charging energy, and capacitances are determined based on the Constant Interaction model, where the total capacitance of a single dot is the sum of the gate, source, and drain capacitances [22, 23]. Additionally, the lateral extent of the dot is inferred by modeling the dot as a circular parallel plate capacitor, from which the radius r can be estimated [24]. These parameters are useful for characterizing the SET as a charge sensor and verifying that the SET quantum dot reasonably matches expectations in terms of size and capacitance. For example, it can be seen from this analysis that the estimated dot radius is around 30 nm, which closely matches expectations for a barrier gate separation of 60 nm.

Parameter	Symbol	Value	Unit
Lever Arm	α	211 ± 4	meV/V
Addition Voltage	V_{add}	70.0 ± 0.7	mV
Charging Voltage	V_C	14.7 ± 0.2	
Total Capacitance	C_{Σ}	11.0 ± 0.2	a F
Gate Capacitance	C_G	2.29 ± 0.02	aF
Source Capacitance	C_S	3.0 ± 0.1	aF
Drain Capacitance	C_D	5.40 ± 0.08	aF
Dot Radius	r	29.8 ± 0.3	nm

Table 1. Device properties estimated based on an analysis of the Coulomb diamonds measured in Figure 3. Values listed are averages across all detected diamonds within a measurement, and errors are the standard deviations of the measured values. Note that $V_C = \alpha V_{\text{add}}$.

4. Discussion

Among the main benefits of using the proposed automated tuning protocol is the time saved compared to tuning SETs heuristically by hand. There remains room to improve the protocol by further reducing the time needed to complete SET tuning and characterization.

The most time-consuming step in the protocol is the 2D sweep or barrier voltages performed in stage 2, taking around 25 minutes for the example shown in Figure 2 (c), compared to around 5 minutes needed to complete all other steps of the tuning process. The speed of acquiring a 2D dataset is limited by the control and readout electronics, namely the DC voltage source, the digital multimeter, and relatively slow communication of both instruments with the computer via GPIB. In contrast, FPGA-based data acquisition systems have been demonstrated with up to 100 MHz signal digitization rates [25], orders of magnitude faster than the electronics used here. A digitizer with an integrated FPGA can perform faster measurements by filling its buffer with the configured number of data points and transferring the block of buffered data to the computer at once. Similarly, an FPGA-controlled voltage source can apply fast voltage sweeps, functioning like an arbitrary waveform generator with 100's of MHz bandwidth. At these high signal generation and acquisition rates, the speed bottleneck may be due to the bandwidth of the low-noise I-V preamplifier. There is always a tradeoff between bandwidth and signal to noise, but use of these fast electronics could reasonably speed up the protocol by a factor ~ 100 .

Besides faster electronics, it may be possible to avoid high resolution 2D sweeps by using a series of cleverly chosen 1D sweeps along different voltage vectors in the barrier-barrier voltage space. With appropriate choice of these vectors, the presence of a Coulomb peak line of suitable angle can be inferred. For example, one vector along the yellow line in Figure 2 (c), in addition to two vectors at around $\pm 20^\circ$ could allow for identification of a number of suitable Coulomb oscillations by interpolating between the detected peaks along each vector. If the initially selected vectors do not reveal linear Coulomb peaks, additional angles can be iteratively added in order to select the bias point in a region free from undesired features (such as those due to unintentional dot confinement or nonuniform density of states in the source/drain leads). The same principle can be applied to the Coulomb diamond measurement for characterization of the SET charge sensor. Instead of a full 2D sweep of the source-

drain and plunger gate voltages, a number of plunger sweeps at different values of V_{SD} could suffice for the determination of the Coulomb diamond geometry. This would make use of interpolation between detected peaks in the various 1D sweeps in order to construct the diamond edges.

Beyond improving time efficiency, the protocol can be refined to improve its robustness to noise and the reliability of its outputs. For example, the results of the 2D barrier sweep can be made more reliable using a machine learning model. The model could predict which regions of the stability diagram correspond to formation of a single central dot as opposed to a dot on the left/right side of the device or an unintentional double dot. Such a model could be trained using the *QFlow* dataset collected by Zwolak, *et. al.* [26] and could utilize various types of neural networks, such as Mask-RCNNs [27]. Furthermore, dynamic feedback [28] could be implemented in order to remain situated at a desired operating point after its selection at the end of stage 3 of the protocol. This would make the device robust to drifts caused by charge rearrangements in the device, allowing it to operate as a useful charge sensor for longer periods of time.

5. Conclusions and Outlook

In this work, we have presented a protocol for automated tuning of SETs (or SHTs) as charge sensors, which can be utilized in a wide variety of applications, such as for performing readout in semiconductor spin qubit systems. The protocol was demonstrated experimentally on an accumulation mode silicon SET device at 1.5 K. This resulted in automated determination of a high-sensitivity operating point, in addition to estimates of key device characteristics, such as dot size and lever arms, based on analysis of Coulomb diamonds. Suggestions for future work are addressed, including improved robustness through machine learning and dynamic feedback, as well as different means of reducing the runtime of the protocol.

Acknowledgments

This research was undertaken thanks in part to funding from the Canada First Research Excellence Fund (Transformative Quantum Technologies) and the Natural Sciences and Engineering Research Council (NSERC) of Canada. This infrastructure would not be possible without the significant contributions of CFREF-TQT, CFI, ISED, the Ontario Ministry of Research and Innovation, and Mike and Ophelia Lazaridis. The authors acknowledge support from the Netherlands Organization of Scientific Research (NWO) under VICI grant VI.C.222.083, European Union's Horizon 2020 and Horizon Europe Research and Innovation Programme under Grant Agreement No. 951852 (QLSI) and No. 101080022 (ONCHIPS).

Author contributions

A.P. developed the tuning protocol and performed the experiments with T.J. A.S., T.J. and J.B. wrote the manuscript. D.B. and Q.T.N. fabricated the devices and T.J. arranged the experiments. F.A.Z. and J.B. contributed equally to supervising the project.

Data availability statement

The data that support the findings of this study are available upon request from the authors.

ORCID iDs

Jonathan Baugh <https://orcid.org/0000-0002-9300-7134>

References

- [1] S. J. Angus, A. J. Ferguson, A. S. Dzurak, and R. G. Clark. A silicon radio-frequency single electron transistor. *Applied Physics Letters*, 92(11):112103, 03 2008.
- [2] Santiago Serrano, MengKe Feng, Wee Han Lim, Amanda E. Seedhouse, Tuomo Tantt, Will Gilbert, Christopher C. Escott, Nikolay V. Abrosimov, Hans-Joachim Pohl, Michael L.W. Thewalt, Fay E. Hudson, Andre Saraiva, Andrew S. Dzurak, and Arne Laucht. Improved single-shot qubit readout using twin rf-set charge correlations. *PRX Quantum*, 5(1), January 2024.
- [3] François Piquemal, Alexandre Bounouh, Laurent Devoille, Nicolas Feltn, O. Thevenot, and Gérard Trapon. Fundamental electrical standards and the quantum metrological triangle. *Comptes Rendus Physique*, 5:857–879, 10 2004.
- [4] D E Feldman and Bertrand I Halperin. Fractional charge and fractional statistics in the quantum hall effects. *Reports on Progress in Physics*, 84(7):076501, June 2021.
- [5] Justyna P. Zwolak and Jacob M. Taylor. Colloquium : Advances in automation of quantum dot devices control. *Reviews of Modern Physics*, 95(1), February 2023.
- [6] Thomas Walter McJunkin. *Heterostructure modifications, fabrication improvements, and measurement automation of Si/SiGe quantum dots for quantum computation*. PhD thesis, Wisconsin U., Madison, 2021.
- [7] J. Darulová, S.J. Pauka, N. Wiebe, K.W. Chan, G.C Gardener, M.J. Manfra, M.C. Cassidy, and M. Troyer. Autonomous tuning and charge-state detection of gate-defined quantum dots. *Physical Review Applied*, 13(5), May 2020.
- [8] T. A. Baart, P. T. Eendebak, C. Reichl, W. Wegscheider, and L. M. K. Vandersypen. Computer-automated tuning of semiconductor double quantum dots into the single-electron regime. *Applied Physics Letters*, 108(21), May 2016.
- [9] Victor Yon, Bastien Galaup, Claude Rohrbacher, Joffrey Rivard, Clément Godfrin, Ruoyu Li, Stefan Kubicek, Kristiaan De Greve, Louis Gaudreau, Eva Dupont-Ferrier, Yann Beilliard, Roger G Melko, and Dominique Drouin. Robust quantum dots charge autotuning using neural network uncertainty. *Machine Learning: Science and Technology*, 5(4):045034, November 2024.
- [10] H. Moon, D. T. Lennon, J. Kirkpatrick, N. M. van Esbroeck, L. C. Camenzind, Liuqi Yu, F. Vigneau, D. M. Zumbühl, G. A. D. Briggs, M. A. Osborne, D. Sejdinovic, E. A. Laird, and N. Ares. Machine learning enables completely automatic tuning of a quantum device faster than human experts. *Nature Communications*, 11(1), August 2020.
- [11] Anton Zubchenko, Danielle Middlebrooks, Torbjørn Rasmussen, Lara Lausen, Ferdinand Kuemmeth, Anasua Chatterjee, and Justyna P. Zwolak. Autonomous bootstrapping of quantum dot devices. *Phys. Rev. Appl.*, 23:014072, Jan 2025.
- [12] Jonas Schuff, Miguel J. Carballido, Madeleine Kotzagiannidis, Juan Carlos Calvo, Marco Caselli, Jacob Rawling, David L. Craig, Barnaby van Straaten, Brandon Severin, Federico Fedele, Simon Svab, Pierre Chevalier Kwon, Rafael S. Egli, Taras Patlatiuk, Nathan Korda, Dominik Zumbühl, and Natalia Ares. Fully autonomous tuning of a spin qubit, 2024.
- [13] N. W. Hendrickx, W. I. L. Lawrie, L. Petit, A. Sammak, G. Scappucci, and M. Veldhorst. A single-hole spin qubit. *Nature Communications*, 11(1), July 2020.
- [14] Denis V. Bulaev and Daniel Loss. Electric dipole spin resonance for heavy holes in quantum dots. *Physical Review Letters*, 98(9), February 2007.
- [15] Brandon Buonacorsi, Benjamin Shaw, and Jonathan Baugh. Simulated coherent electron shuttling in silicon quantum dots. *Physical Review B*, 102(12), September 2020.
- [16] A. J. Sousa de Almeida, A. Márquez Seco, T. van den Berg, B. van de Ven, F. Bruijnes, S. V. Amitonov, and F. A. Zwanenburg. Ambipolar charge sensing of few-charge quantum dots. *Phys. Rev. B*, 101:201301, May 2020.

- [17] Andrija Paurevic. Quantum dot control. <https://github.com/mainCSG/QuantumDotControl>, 2024.
- [18] L. M. K. Vandersypen, H. Bluhm, J. S. Clarke, A. S. Dzurak, R. Ishihara, A. Morello, D. J. Reilly, L. R. Schreiber, and M. Veldhorst. Interfacing spin qubits in quantum dots and donors—hot, dense, and coherent. *npj Quantum Information*, 3(1), September 2017.
- [19] Blake M. Freeman, Joshua S. Schoenfeld, and HongWen Jiang. Comparison of low frequency charge noise in identically patterned Si/SiO₂ and Si/SiGe quantum dots. *Applied Physics Letters*, 108(25):253108, 06 2016.
- [20] L. Petit, J. M. Boter, H. G. J. Eenink, G. Droulers, M. L. V. Tagliaferri, R. Li, D. P. Franke, K. J. Singh, J. S. Clarke, R. N. Schouten, V. V. Dobrovitski, L. M. K. Vandersypen, and M. Veldhorst. Spin lifetime and charge noise in hot silicon quantum dot qubits. *Phys. Rev. Lett.*, 121:076801, Aug 2018.
- [21] Nard Dumoulin Stuyck, Roy Li, Stefan Kubicek, Fahd A. Mohiyaddin, Julien Jussot, B. T. Chan, George Simion, Bogdan Govoreanu, Marc Heyns, and Iuliana Radu. An integrated silicon mos single-electron transistor charge sensor for spin-based quantum information processing. *IEEE Electron Device Letters*, 41(8):1253–1256, 2020.
- [22] LP Kouwenhoven, CM Marcus, PL McEuen, S Tarucha, RM Westervelt, and NS Wingreen. Electron transport in quantum dots. In LP Kouwenhoven and GB Schon, editors, *NATO-ASI Workshop on Mesoscopic Electron Transport*, pages 105–214, 1997.
- [23] R. Hanson, L. P. Kouwenhoven, J. R. Petta, S. Tarucha, and L. M. K. Vandersypen. Spins in few-electron quantum dots. *Reviews of Modern Physics*, 79(4):1217–1265, October 2007.
- [24] S. D. Liles, R. Li, C. H. Yang, F. E. Hudson, M. Veldhorst, A. S. Dzurak, and A. R. Hamilton. Spin and orbital structure of the first six holes in a silicon metal-oxide-semiconductor quantum dot. *Nature Communications*, 9(1), August 2018.
- [25] Timo Haarman, Antonio Sousa de Almeida, Amber Heskes, Floris Zwanenburg, and Nikolaos Alachiotis. Fpga-accelerated quantum transport measurements. In *2023 International Conference on Field Programmable Technology (ICFPT)*, pages 44–52, 2023.
- [26] Justyna P. Zwolak, Joshua Ziegler, Sandesh S. Kalantre, and Jacob M. Taylor. Qflow 2.0: Quantum dot data for machine learning, national institute of standards and technology, 2022.
- [27] Andrija Paurevic. Automated Tuning and Optimal Control of Spin Qubits in Quantum Dot Devices. Master’s thesis, U. Waterloo (main), 2024.
- [28] C. H. Yang, W. H. Lim, F. A. Zwanenburg, and A. S. Dzurak. Dynamically controlled charge sensing of a few-electron silicon quantum dot. *AIP Advances*, 1(4), October 2011.